

Thermodynamics of the $O(3)$ model in 1+1 dimensions: lattice vs. analytical results

Elina Seel,^a Dominik Smith,^{abc} Stefano Lottini,^a Francesco Giacosa^a

^a*Institut für Theoretische Physik, Johann Wolfgang Goethe-Universität,
Max-von-Laue-Str. 1, 60438 Frankfurt am Main, Germany*

^b*Technische Universität Darmstadt, Institut für Kernphysik,
Schlossgartenstr. 2, 64289 Darmstadt, Germany*

^c*Fakultät für Physik, Universität Bielefeld, 33615 Bielefeld, Germany*

E-mail: seel, smith, lottini, giacosa@th.physik.uni-frankfurt.de

ABSTRACT: A detailed study of the thermodynamics of the $O(N = 3)$ model in 1+1 dimensions is presented, employing a two-particle-irreducible resummation prescription as well as fully nonperturbative finite-temperature lattice simulations. The analytical results are computed using the Cornwall-Jackiw-Tomboulis (CJT) formalism and the auxiliary field method to one- and to two-loop order. The lattice results are obtained through Monte Carlo simulation for various lattice spacings. The analytical and lattice results for pressure, trace anomaly, and energy density, resembling closely those of four-dimensional Yang-Mills theories, are compared with each other. We find that to one-loop order there is a good correspondence between the CJT formalism and the lattice study for low temperatures. However, at high T the two-loop calculation fares better, correcting for the overestimation from the former approximation.

KEYWORDS: $O(3)$ model, CJT formalism, lattice thermodynamics, low-dimensional models

Contents

1	Introduction	1
2	The model and the analytic results	3
2.1	Generating functional	3
2.2	The CJT effective potential	4
2.3	One-loop approximation	6
2.4	Regularisation	8
2.5	Renormalisation	8
2.6	Two-loop approximation	9
3	Lattice simulation	13
3.1	Thermodynamical observables	14
3.2	Scale setting	15
3.3	Numerical results	16
3.3.1	Beta-function	16
3.3.2	Thermodynamics	16
4	Comparison of analytical and lattice results	18
5	Summary	21
A	Algorithms and autocorrelations	23

1 Introduction

As discussed by Polyakov [1], the two-dimensional $O(N)$ nonlinear sigma model has interesting features in common with four-dimensional non-Abelian gauge theories. For these reasons it has been investigated in the past as a suitable toy model for QCD, see Refs. [2–7] and refs. therein. Remarkably, the two-dimensional $O(3)$ model emerges also naturally as a particular subsystem of four-dimensional theories: see Ref. [8], in which the dual Meissner mechanism for confinement is investigated in the framework of supersymmetric QCD.

In 1+1 dimensions, the coupling constant is dimensionless, the theory is renormalisable both perturbatively and in the $1/N$ expansion, and has also a negative beta-function, thus showing asymptotic freedom [1]. Moreover, the two-dimensional $O(N)$ model is conformally invariant at the classical level, but, just as Yang-Mills theories in four dimensions, at the quantum level an energy scale emerges due to quantum corrections (trace anomaly). In fact, it exhibits a nonperturbative mass gap $m = \mu \exp(-2\pi/g^2)$ generated dynamically due to the interactions, where g is the coupling constant and μ the renormalisation parameter.

Note that: (i) since the mass is non-analytic for $g \rightarrow 0$, it vanishes in perturbation theory; (ii) unlike the case of more than two dimensions, here no spontaneous breaking of the global $O(N)$ symmetry takes place: this is related to the Mermin-Wagner-Coleman theorem [9, 10], which forbids spontaneous breaking of a continuous global symmetry in a $(1 + 1)$ -dimensional homogeneous system at any temperature.

The effective potential at zero temperature has been investigated in Refs. [11, 12]. In Ref. [13] the model was studied at finite temperature in perturbation theory and to leading order (LO) in the large- N limit; this was subsequently extended in Refs. [6, 7] to next-to-leading order (NLO) in the $1/N$ expansion. It is found that the NLO effective potential contains temperature-dependent divergences. Fortunately, it turns out that the effective potential can still be renormalised at the minimum.

In this work we study the nonlinear $O(N = 3)$ model in $1+1$ dimensions at nonzero temperature both analytically and numerically. On the analytical side, we compute the thermodynamic properties by employing the Cornwall-Jackiw-Tomboulis (CJT) formalism [14] and using the auxiliary field method in the one- and two-loop approximation. We present analytical expressions for the renormalised pressure, the trace anomaly, the energy density, and the quasi-particle mass of the scalar fields. On the numerical side, we compute the thermodynamic quantities via “first-principles” Monte Carlo lattice calculation using the so called “integral method”. We then compare the analytic and the lattice results: at one loop, a good agreement is found for small temperatures, but the analytic result for the pressure is too large when T increases. When going to the two-loop approximation, a considerable improvement in the high- T domain is obtained.

Among the motivations of the present study are the following. (i) A check of the validity of the CJT formalism: through the direct comparison with our precise lattice results we test to which extent the widely used CJT theoretical approach gives reliable results for thermodynamic quantities such as pressure and energy density. No free parameter can be adjusted when doing this comparison. (ii) Lattice evaluation: the two-dimensional $O(N = 3)$ model has been already studied in a variety of lattice-related contexts (see Section 3 for references), but to our knowledge a systematic evaluation of all thermodynamic quantities was not yet presented. The lattice results are interesting on their own, and can be used by other groups who study this system. (iii) Due to the mentioned similarity between the two-dimensional $O(N)$ model and gauge theories, we aim at a better understanding of fundamental issues such as the nonperturbative mass generation through the trace anomaly and its behaviour when the temperature is raised: the link between a non-perturbative vacuum and a perturbative high-temperature domain is non-trivial.

A further interesting motivation for the study of the present model is that, for the choice $N = 3$, the model exhibits instantonic solutions both at zero [2] and nonzero temperature [15, 16]. In fact, the $O(3)$ model in $1 + 1$ dimensions is topologically equivalent to the CP^1 model, whereas CP^{n-1} theories admit instantons for each value of n [17, 18]. The instanton solutions are topologically nontrivial field configurations localised in space and time, associated to classical, finite-action solutions of Euclidean field equations. They give rise to tunneling processes between different classical vacua [19]. For this reason they have been regarded in the framework of Yang-Mills theories $SU(N > 1)$ (see for instance [5, 20–

[22] and refs. therein) as a possible crucial ingredient for understanding nonperturbative properties, such as confinement and the emergence of a mass gap.

Finally, one may wonder what is the role of instantons and calorons in the thermodynamics of this model; although our analytical method does not distinguish topologically trivial and nontrivial field configurations, we suspect, in agreement with [23], that the role of instantons and/or calorons can be relevant.

The manuscript is organised as follows: in Sec. 2 we present the model, derive the effective potential to one- and two-loop order, and derive the analytic expressions for pressure, trace anomaly and energy density. In Sec. 3 we present a detailed lattice study of the model. In Sec. 4 we show and discuss the comparison of analytic and lattice results. The reader interested only in the results may skip the details of Secs. 2 and 3 and go directly to Sec. 4. Finally, conclusions and outlooks are described in Sec. 5.

Throughout the paper, we will use natural units $\hbar = c = k_B \equiv 1$. All computations at nonzero temperature T are done in the imaginary-time formalism, with the shorthand

$$\int_K f(K) \equiv T \sum_{n=-\infty}^{+\infty} \int \frac{dk}{(2\pi)} f(k, 2\pi nT) \ , \quad (1.1)$$

where we have used the Euclidean momentum $K = (k_x = k, k_\tau)$.

2 The model and the analytic results

2.1 Generating functional

The nonlinear $O(N)$ model in 1 + 1 dimensions at nonzero temperature is defined by the following generating functional:

$$\mathcal{Z} = \mathcal{N} \int \mathcal{D}\Phi \delta \left[\Phi^2 - \frac{N}{g^2} \right] \exp \left(- \int_0^{1/T} d\tau \int_{-\infty}^{\infty} dx \mathcal{L}_0 \right) \ , \quad (2.1)$$

where g is the dimensionless coupling constant. The N fields of the model are contained in the column matrix Φ , which for future purposes we write as

$$\Phi^t = (\sigma, \pi_1, \dots, \pi_{N-1}) \ . \quad (2.2)$$

Moreover, we also use the notation $\Phi^2 = \Phi^t \Phi$ and $\vec{\pi}^t = (\pi_1, \dots, \pi_{N-1})$.

The Lagrangian \mathcal{L}_0 entering Eq. (2.1) is a simple Lagrangian for N massless scalar fields, which in Euclidean space reads:

$$\mathcal{L}_0 = \frac{1}{2} (\partial_\mu \Phi)^2 \ , \quad (2.3)$$

with $\partial_1 = \partial_x$, $\partial_2 = \partial_\tau$.

Due to the δ -function entering the partition function (2.1) the fields of the model are constrained by the condition

$$\Phi^2 = \frac{N}{g^2} \ . \quad (2.4)$$

This nonlinear constraint enforces the N degrees of freedom of the model on an $(N - 1)$ -dimensional hypersphere and induces interactions between them. Using the mathematically well-defined (i.e. convergent) form of the usual representation of the functional δ -function

$$\delta \left[\Phi^2 - \frac{N}{g^2} \right] \sim \lim_{\varepsilon \rightarrow 0^+} \int \mathcal{D}\alpha \exp \left\{ - \int_0^{1/T} d\tau \int_{-\infty}^{+\infty} dx \left[\frac{i\alpha}{2} \left(\Phi^2 - \frac{N}{g^2} \right) + \frac{N\varepsilon}{8} \alpha^2 \right] \right\} , \quad (2.5)$$

the generating functional and the corresponding Lagrangian can be rewritten as follows:

$$\mathcal{Z} = \lim_{\varepsilon \rightarrow 0^+} \mathcal{N}' \int \mathcal{D}\alpha \mathcal{D}\Phi \exp \left(- \int_0^{1/T} d\tau \int_{-\infty}^{\infty} dx \mathcal{L} \right) , \quad (2.6)$$

where

$$\begin{aligned} \mathcal{L} &= \frac{1}{2}(\partial_\mu \Phi)^2 + U(\Phi, \alpha) ; \\ U(\Phi, \alpha) &= \frac{i}{2}\alpha \left(\Phi^2 - \frac{N}{g^2} \right) + \frac{N\varepsilon}{8} \alpha^2 . \end{aligned} \quad (2.7)$$

In the last expression α is an unphysical auxiliary field serving as a Lagrange multiplier. In the next Subsections we shall use the form in Eqs. (2.6) and (2.7) for our explicit calculation of the thermodynamical properties. Interestingly, by further eliminating α we obtain the following equivalent form of the generating functional:

$$\mathcal{Z} = \lim_{\varepsilon \rightarrow 0^+} \tilde{\mathcal{N}} \int \mathcal{D}\Phi \exp \left\{ - \int_0^{1/T} d\tau \int_{-\infty}^{\infty} dx \left[\frac{1}{2}(\partial_\mu \Phi)^2 + \frac{(\Phi^2 - N/g^2)^2}{2N\varepsilon} \right] \right\} , \quad (2.8)$$

in which the ‘‘infinitely steep’’ mexican-hat form of the potential is evident.

2.2 The CJT effective potential

In order to compute thermodynamic quantities we use the CJT formalism [14] which is a self-consistent resummation prescription to compute the effective potential for a given theory (see also e.g. Refs. [24–32]).

The first step consists in shifting the fields σ and α by their nonvanishing vacuum expectation values,

$$\sigma \rightarrow \phi + \sigma , \quad \alpha \rightarrow \alpha_0 + \alpha . \quad (2.9)$$

As a consequence, the Lagrangian (2.7) takes the form

$$\mathcal{L} = \frac{1}{2}(\partial_\mu \Phi)^2 + \frac{N\varepsilon}{8}(\alpha_0 + \alpha)^2 + \frac{i}{2}(\alpha_0 + \alpha) \left(\sigma^2 + \vec{\pi}^2 + 2\sigma\phi + \phi^2 - \frac{N}{g^2} \right) . \quad (2.10)$$

As one can see from Eq. (2.10) this shift produces a bilinear mixing term, $i\alpha\sigma\phi$, which renders the propagator matrix non-diagonal in the fields σ and α . There are two possible ways to handle the ensuing mixing. One is to keep this term and allow for a non-diagonal propagator which mutually transforms the fields σ and α into each other [24, 33]. The

second way, used in this work and based on the study of Ref. [25], consists in performing the shift

$$\alpha \longrightarrow \alpha - 4 \frac{i\phi}{N\varepsilon} \sigma , \quad (2.11)$$

which eliminates the mixing term. In Ref. [25] it was explicitly demonstrated up to two-loop order that these two methods to handle the mixing term are equivalent, i.e. they yield the same results for the effective potential and for the gap equations. However, the shift introduced in Eq. (2.11) considerably simplifies the calculations. From the resulting Lagrangian,

$$\begin{aligned} \mathcal{L} = & \frac{1}{2} (\partial_\mu \sigma)^2 + \frac{1}{2} (\partial_\mu \pi_i)^2 + \frac{1}{2} \left(i\alpha_0 + \frac{4\phi^2}{N\varepsilon} \right) \sigma^2 + \frac{1}{2} (i\alpha_0) \pi_i^2 + \frac{1}{2} \frac{N\varepsilon}{4} \alpha^2 \\ & + \frac{i}{2} \alpha (\sigma^2 + \pi_i^2) + \frac{2\phi}{N\varepsilon} \sigma (\sigma^2 + \pi_i^2) + U(\phi, \alpha_0) , \end{aligned} \quad (2.12)$$

one can immediately deduce the inverse tree-level propagators and the tree-level masses:

$$D_i^{-1}(K; \phi, \alpha_0) = K^2 + m_i^2 , \quad i = \sigma, \vec{\pi}; \quad (2.13)$$

$$m_\sigma^2 = i\alpha_0 + \frac{4\phi^2}{N\varepsilon} ; \quad m_\pi^2 = i\alpha_0 ; \quad (2.14)$$

$$D_\alpha^{-1} = m_\alpha^2 = \frac{N\varepsilon}{4} . \quad (2.15)$$

Within the aforementioned CJT formalism the standard expression for the effective potential is given by

$$\begin{aligned} V_{\text{eff}} \equiv V_{\text{eff}}(\phi, \alpha_0; G_\sigma, G_\pi, G_\alpha) = \\ U(\phi, \alpha_0) + \sum_{i=\sigma, \vec{\pi}, \alpha} \frac{1}{2} \int_K [\ln G_i^{-1}(K) + D_i^{-1}(K; \phi, \alpha_0) G_i(K) - 1] + V_2 , \end{aligned} \quad (2.16)$$

where $U(\phi, \alpha_0)$ is the tree-level potential just as in Eq. (2.7), $D_i(K; \phi, \alpha_0)$ are the tree-level propagators, $G_i(K)$ are the full propagators in momentum space and V_2 contains all two-particle-irreducible (2PI) self-interaction terms. The full propagators and the condensates are evaluated by using the stationary conditions for the effective potential:

$$\frac{\delta V_{\text{eff}}}{\delta \phi} = 0 , \quad \frac{\delta V_{\text{eff}}}{\delta \alpha_0} = 0 , \quad \frac{\delta V_{\text{eff}}}{\delta G_i(K)} = 0 ; \quad i = \sigma, \vec{\pi}, \alpha . \quad (2.17)$$

For the full propagators one obtains

$$G_i^{-1}(K) = K^2 + M_i^2 ; \quad M_i^2 = m_i^2 + \Sigma_i , \quad (2.18)$$

where Σ_i denotes the self-energy

$$\Sigma_i = 2 \frac{\delta V_2}{\delta G_i(K)} . \quad (2.19)$$

2.3 One-loop approximation

Restricting to one-loop order, the 2PI contribution to the effective potential is equal to zero, $V_2 \equiv 0$. Thus, the effective potential is given by:

$$V_{\text{eff}} = \frac{i}{2}\alpha_0 \left(\phi^2 - \frac{N}{g^2} \right) + \frac{N\varepsilon}{8}\alpha_0^2 + \frac{1}{2} \sum_{i=\sigma, \bar{\pi}, \alpha} \int_K [\ln G_i^{-1}(K) + D_i^{-1}(K; \phi, \alpha_0)G_i(K) - 1] . \quad (2.20)$$

Using the stationary conditions (2.17) one derives the following equations for the two condensates:

$$0 = \phi \left(i\alpha_0 + \frac{4}{N\varepsilon} \int_K G_\sigma(K) \right) ; \quad (2.21)$$

$$i\alpha_0 = \frac{2}{N\varepsilon} \left[\phi^2 - \frac{N}{g^2} + \int_K G_\sigma(K) + (N-1) \int_k G_\pi(K) \right] , \quad (2.22)$$

and for the full propagators:

$$G_i^{-1}(K) = K^2 + M_i^2 = D_i^{-1}(K; \phi, \alpha_0) ; \quad (2.23)$$

$$M_i^2 = m_i^2 + \Sigma_i = m_i^2 . \quad (2.24)$$

In fact, since $V_2 = 0$, the self-energy Σ_i vanishes in the one-loop approximation. Substituting the right hand side of Eq. (2.22) for $i\alpha_0$ gives the following equations for the physical condensate ϕ and for the masses:

$$0 = \phi \left(M_\pi^2 + \frac{4}{N\varepsilon} \int_K G_\sigma(K) \right) ; \quad (2.25)$$

$$M_\sigma^2 = M_\pi^2 + \frac{4\phi^2}{N\varepsilon} ; \quad (2.26)$$

$$M_\pi^2 = \frac{2}{N\varepsilon} \left[\phi^2 - \frac{N}{g^2} + \int_K G_\sigma(K) + (N-1) \int_K G_\pi(K) \right] . \quad (2.27)$$

We now study separately the cases $\phi \neq 0$ and $\phi = 0$ and show that, in the present two-dimensional model, the latter holds.

- (i) We assume $\phi \neq 0$ (corresponding to spontaneous symmetry breaking). When taking the limit $\varepsilon \rightarrow 0^+$ the degree of freedom denoted by σ becomes frozen due to an infinitely heavy mass, see Eq. (2.26):

$$\lim_{\varepsilon \rightarrow 0^+} M_\sigma^2 = \lim_{\varepsilon \rightarrow 0^+} \frac{4\phi^2}{N\varepsilon} = \infty , \quad (2.28)$$

from which it follows that

$$\lim_{\varepsilon \rightarrow 0^+} \frac{1}{\varepsilon} \int_K G_\sigma(K) = 0 . \quad (2.29)$$

Moreover, from Eq. (2.25) we obtain that $M_\pi = 0$. Then, the gap equation (2.27) becomes:

$$\phi^2 = \frac{N}{g^2} - (N-1) \int_K G_\pi(K) = \frac{N}{g^2} - (N-1) \int_0^\infty \frac{dk}{\pi} \frac{1}{k [\exp(k/T) - 1]} . \quad (2.30)$$

There is no solution to this equation since the integral in the right-hand side is divergent, whereas $\phi^2 - N/g^2$ is finite. Thus, the case $\phi \neq 0$ leads to inconsistencies and cannot hold. This means that in two dimensions there is no spontaneous symmetry breaking of the global $O(N)$ symmetry of the nonlinear $O(N)$ model, in agreement with the Mermin-Wagner-Coleman theorem mentioned in the Introduction. Note that in four dimensions this would have not been the case: a condensation of ϕ would take place signalling an explicit breaking of chiral symmetry, see for instance Refs. [25, 26, 34].

- (ii) We set $\phi = 0$ (no spontaneous symmetry breaking). In this case Eq. (2.25) is trivially fulfilled. Eq. (2.26) implies that the masses of σ and π become degenerate,

$$M_\sigma^2 = M_\pi^2 \equiv M^2 \quad , \quad (2.31)$$

so that

$$G_\pi(K) = G_\sigma(K) \equiv G(K) \quad . \quad (2.32)$$

Then, from Eq. (2.27) we find

$$\frac{N}{g^2} = N \int_K G(K) = N \int_0^\infty \frac{dk}{\pi} \frac{n[\omega_k(M)]}{\omega_k(M)} \quad , \quad (2.33)$$

where

$$\omega_k(M) = \sqrt{k^2 + M^2} \quad (2.34)$$

and

$$n[\omega_k(M)] = \{\exp[\omega_k(M)/T] - 1\}^{-1} \quad . \quad (2.35)$$

From the previous equation one can determine the behaviour of the function $M(T)$, see later. The case $\phi = 0$ does not lead to any inconsistencies and is the realised one. It should be stressed that this solution is highly nontrivial: instead of two massless degrees of freedom one has in the vacuum three equally massive particles.

The basic quantity for a thermodynamic study of the system is the pressure, which is, up to a sign, identical to the minimum of the effective potential,

$$p = -V_{\text{eff}}^{\text{min}} \quad .$$

From the pressure we can compute the energy density ϵ and the trace anomaly θ using the first principle of thermodynamics:

$$\begin{aligned} \epsilon &= T \frac{dp}{dT} - p \quad ; \\ \theta &= \epsilon - p \quad . \end{aligned}$$

2.4 Regularisation

The nonlinear $O(N)$ model is infrared-finite, since the mass is nonvanishing. Thus, there are only ultraviolet divergences, which we regularise via an ultraviolet cutoff Λ [2, 6, 7]:

$$\int_K G(K) = \int_0^\Lambda \frac{dk}{\pi} \frac{n[\omega_k(M)]}{\omega_k(M)} + \frac{1}{4\pi} \ln \frac{\Lambda^2}{M^2} ; \quad (2.36)$$

$$\int_K \ln G^{-1}(K) = -2 \int_0^\Lambda \frac{dk}{\pi} \frac{k^2}{\omega_k(M)} \frac{n[\omega_k(M)]}{\omega_k(M)} + \frac{M^2}{4\pi} \left(1 + \ln \frac{\Lambda^2}{M^2} \right) , \quad (2.37)$$

where we subtracted divergent M - and T -independent terms. In the previous equations the quantity $M = M(T)$ denotes the temperature-dependent mass. At $T = 0$ one has $M(T = 0) = m$, with m being the only dimensionful parameter of the model (emerging through dimensional transmutation) — see the next Subsection for further details.

Using equations (2.16) and (2.37) we obtain the regularised effective potential and the regularised pressure:

$$p_{\text{reg}} \equiv p_{\text{reg}}(T) = \frac{NM^2}{2g^2} + N \int_0^\Lambda \frac{dk}{\pi} \frac{k^2}{\omega_k(M)} \frac{n[\omega_k(M)]}{\omega_k(M)} - \frac{NM^2}{8\pi} \left(1 + \ln \frac{\Lambda^2}{M^2} \right) , \quad (2.38)$$

where the regularised mass $M = M(T)$ is determined from

$$\frac{N}{g^2} = N \int_0^\Lambda \frac{dk}{\pi} \frac{n[\omega_k(M)]}{\omega_k(M)} + \frac{N}{4\pi} \ln \frac{\Lambda^2}{M^2} . \quad (2.39)$$

Note that at $T = 0$ we obtain the following relation:

$$\frac{N}{g^2} = \frac{N}{4\pi} \ln \frac{\Lambda^2}{m^2} . \quad (2.40)$$

2.5 Renormalisation

After regularisation we can perform the renormalisation. First, we compute the renormalised coupling constant as it was defined in [2]:

$$\begin{aligned} \frac{1}{g_{\text{ren}}^2} &= \frac{2}{N} \left. \frac{dp_{\text{reg}}(T=0)}{dm^2} \right|_{m^2=\mu^2} \\ &= \frac{2}{N} \frac{d}{dm^2} \left[N \frac{m^2}{2g^2} - N \frac{m^2}{8\pi} \left(1 + \ln \frac{\Lambda^2}{m^2} \right) \right]_{m^2=\mu^2} = \frac{1}{g^2} - \frac{1}{4\pi} \ln \frac{\Lambda^2}{\mu^2} . \end{aligned} \quad (2.41)$$

Inserting this result in Eq. (2.38) and subtracting the zero-temperature contribution $-Nm^2/8\pi$ we get the renormalised pressure in the limit $\Lambda \rightarrow \infty$:

$$\begin{aligned} p_{\text{ren}} &= \frac{NM^2}{2g^2} + N \int_0^\infty \frac{dk}{\pi} \frac{k^2}{\omega_k(M)} \frac{n[\omega_k(M)]}{\omega_k(M)} - \frac{NM^2}{8\pi} \left(1 + \ln \frac{\Lambda^2}{M^2} \right) + \frac{Nm^2}{8\pi} = \\ &= \frac{NM^2}{2g_{\text{ren}}^2} + N \int_0^\infty \frac{dk}{\pi} \frac{k^2}{\omega_k(M)} \frac{n[\omega_k(M)]}{\omega_k(M)} - \frac{NM^2}{8\pi} \left(1 + \ln \frac{\mu^2}{M^2} \right) + \frac{Nm^2}{8\pi} , \end{aligned} \quad (2.42)$$

where we have used Eq. (2.40). The temperature-dependent mass M is determined from the renormalised gap equation:

$$\begin{aligned}\frac{1}{g^2} &= \frac{1}{g_{\text{ren}}^2} + \frac{1}{4\pi} \ln \frac{\Lambda^2}{\mu^2} = \int_0^\infty \frac{dk}{\pi} \frac{n[\omega_k(M)]}{\omega_k(M)} + \frac{1}{4\pi} \ln \frac{\Lambda^2}{M^2} ; \\ \frac{1}{g_{\text{ren}}^2} &= \int_0^\infty \frac{dk}{\pi} \frac{n[\omega_k(M)]}{\omega_k(M)} + \frac{1}{4\pi} \ln \frac{\mu^2}{M^2} .\end{aligned}\quad (2.43)$$

Solving Eq. (2.43) at $T = 0$ one can show that the model exhibits dimensional transmutation, meaning that there is a nonvanishing mass parameter m in the vacuum which is generated due to the renormalisation of quantum corrections:

$$M^2(T = 0) = m^2 = \mu^2 \exp\left(-\frac{4\pi}{g_{\text{ren}}^2}\right) . \quad (2.44)$$

Notice that m depends non-analytically on the coupling constant for $g \rightarrow 0$. Thus, the mass would vanish if naive perturbation theory were applied.

In order to determine the asymptotic behaviour of the theory we compute the beta-function of the running coupling:

$$\begin{aligned}\mu \frac{dg_{\text{ren}}^2}{d\mu} &= \mu \frac{d}{d\mu} \left[g^2 \left(1 - \frac{g^2}{4\pi} \ln \frac{\Lambda^2}{\mu^2} \right)^{-1} \right] = \\ &= -\frac{1}{2\pi} \left[g^2 \left(1 - \frac{g^2}{4\pi} \ln \frac{\Lambda^2}{\mu^2} \right)^{-1} \right]^2 = -\frac{g_{\text{ren}}^4}{2\pi} < 0 .\end{aligned}\quad (2.45)$$

We have shown that the coupling constant decreases with increasing μ and thus the theory is asymptotically free.

2.6 Two-loop approximation

The Lagrangian (2.12) contains only three-point interaction terms and no four-point vertices. Therefore to two-loop order we can only construct sunset diagrams but no double-bubbles. Besides, since there is no spontaneous symmetry breaking in two dimensions, i.e. $\phi = 0$ and $M_\sigma^2 = M_\pi^2 = M^2$, only the term $i\alpha(\sigma^2 + \pi_i^2)/2$ contributes to the 2PI part of the effective potential via a sunset diagram:

$$V_2 = \frac{N}{4} \int_K \int_P G_\alpha(K+P)G(K)G(P) . \quad (2.46)$$

Taking the sunset diagram into account the effective potential to two-loop order is:

$$\begin{aligned}V_{\text{eff}}(\alpha_0, G, G_\alpha) &= N \frac{i\alpha_0}{2g^2} + \frac{N\varepsilon}{8} \alpha_0^2 \\ &+ \frac{1}{2} \sum_{i=\sigma, \vec{\pi}, \alpha} \int_K [\ln G_i^{-1}(K) + D_i^{-1}(K; \alpha_0)G_i(K) - 1] + V_2 .\end{aligned}\quad (2.47)$$

The corresponding equations for the condensate of the auxiliary field and for the full propagators are:

$$i\alpha_0 = \frac{2}{N\varepsilon} \left(-\frac{1}{g^2} + \int_K G(K) \right) ; \quad (2.48)$$

$$G^{-1}(K) = D^{-1}(K) + \Sigma(K) ; \quad (2.49)$$

$$G_\alpha^{-1}(K) = D_\alpha^{-1}(K) + \Sigma_\alpha(K) , \quad (2.50)$$

where the self-energies for α and for the N scalar fields read

$$\Sigma(K) = \frac{2}{N} \frac{\delta V_2}{\delta G(K)} = \int_P G(P) G_\alpha(K-P) ; \quad (2.51)$$

$$\Sigma_\alpha(K) = 2 \frac{\delta V_2}{\delta G_\alpha(K)} = \frac{N}{2} \int_P G(P) G(K-P) . \quad (2.52)$$

The temperature-dependent mass of the scalar fields is determined by solving

$$M^2 = m^2 + \text{Re} \Sigma = i\alpha_0 + \text{Re} \int_P G(P) G_\alpha(K-P) , \quad (2.53)$$

where we have used $m^2 = i\alpha_0$, see Eq. (2.14). Besides, using Eq. (2.15) we obtain the following relation for the full propagator of the auxiliary field:

$$G_\alpha^{-1}(K) = \frac{N\varepsilon}{4} + \frac{N}{2} \int_P G(P) G(K-P) . \quad (2.54)$$

Next, we perform the following three steps to simplify these results:

- (i) Out of Eqs. (2.48), (2.53), and (2.54) we obtain

$$\begin{aligned} -\frac{1}{g^2} + \int_K G(K) &= 2\varepsilon \left[M^2 - \text{Re} \int_P G(P) G_\alpha(K-P) \right] \\ &= 2\varepsilon \left[M^2 - \text{Re} \int_P \frac{G(P)}{\frac{N\varepsilon}{4} + \frac{N}{2} \int_L G(L) G(K-P-L)} \right] . \end{aligned} \quad (2.55)$$

In the nonlinear limit $\varepsilon \rightarrow 0^+$ this expression reduces to

$$\begin{aligned} \frac{1}{g^2} &= \int_K G(K) = \int_K \frac{1}{K^2 + i\alpha_0 + \int_P G(P) G_\alpha(K-P)} \\ &= \int_K \frac{1}{K^2 + M^2 + \text{Im} \int_P G(P) G_\alpha(K-P)} , \end{aligned} \quad (2.56)$$

where the real part of the sunset has been reabsorbed in the definition of the mass, see Eq. (2.53). Moreover, since all three particles have the same mass and decays are strongly suppressed, we neglect the imaginary part of the self-energy:

$$\text{Im} \left[\int_P G(P) G_\alpha(K-P) \right] = 0 . \quad (2.57)$$

Then, we obtain at two-loop order the same gap equation as in the one-loop approximation:

$$\frac{1}{g^2} = \int_K G(K) ; \quad (2.58)$$

this result is consistent with the observation that the next-to-leading-order effective potential is minimised by the leading-order mass [6, 7, 11].

- (ii) Furthermore, using Eqs. (2.15) and (2.54) one can show that in the nonlinear limit the two integrals $\int_K D_\alpha^{-1} G_\alpha(K) - 1$ and $\int_K \int_P G_\alpha(K+P)G(K)G(P)$, involving the auxiliary field appearing in the effective potential (2.47), reduce to constant terms which are irrelevant for the thermodynamics:

$$\int_K D_\alpha^{-1} G_\alpha(K) - 1 = \frac{\frac{N\varepsilon}{4}}{\frac{N\varepsilon}{4} + \frac{N}{2} \int_P G(P)G(K-P)} - 1 \stackrel{\varepsilon \rightarrow 0^+}{=} -1 .$$

Similarly, we get (at the minimum):

$$\begin{aligned} V_2^{\min} &= \frac{N}{4} \int_K \int_P G_\alpha(K)G(P)G(K+P) \\ &= \frac{N}{4} \int_K \frac{1}{\frac{N\varepsilon}{4} + \frac{N}{2} \int_L G(L)G(K-L)} \int_P G(P)G(K+P) \\ &\stackrel{\varepsilon \rightarrow 0^+}{=} \frac{N}{4} \int_K \frac{1}{\frac{N}{2} \int_L G(L)G(K-L)} \int_P G(P)G(K+P) \\ &\stackrel{L=-Q}{=} \frac{N}{4} \int_K \frac{1}{\frac{N}{2} \int_{-Q} G(Q)G(K+Q)} \int_P G(P)G(K+P) \\ &= \frac{N}{4} \int_K \frac{1}{\frac{N}{2} \int_Q G(Q)G(K+Q)} \int_P G(P)G(K+P) = \text{const.} \quad (2.59) \end{aligned}$$

- (iii) Finally, we can rewrite the term $\int_K [D^{-1}(K; \alpha_0)G(K) - 1]$ as follows:

$$\begin{aligned} \int_K [D^{-1}(K; \alpha_0)G(K) - 1] &= \int_K \left[\frac{K^2 + m^2}{K^2 + M^2} - 1 \right] = \quad (2.60) \\ &= \int_K \frac{m^2 - M^2}{K^2 + M^2} = (m^2 - M^2) \int_K G(K) = \frac{(m^2 - M^2)}{g^2} , \end{aligned}$$

where we used the gap equation (2.58). Besides, we set $D^{-1}(K; \alpha_0) = K^2 + i\alpha_0 = K^2 + m^2$.

Using the results obtained in (i), (ii) and (iii) the effective potential to two-loop order simplifies as follows:

$$V_{\text{eff}}^{\min} = -\frac{NM^2}{2g^2} + \frac{N}{2} \int_K \ln G^{-1}(K) + \frac{1}{2} \int_K \ln G_\alpha^{-1}(K) . \quad (2.61)$$

At $T = 0$ the effective potential can be regularised analytically. Introducing an ultra-violet momentum cutoff and dropping m -independent divergences one obtains [2, 6, 7]:

$$\begin{aligned} V_{\text{eff}}(T = 0) &= -\frac{Nm^2}{2g^2} + \frac{Nm^2}{8\pi} \left(1 + \ln \frac{\Lambda^2}{m^2} \right) \quad (2.62) \\ &+ \frac{1}{8\pi} \left[(\Lambda^2 + 2m^2) \ln \ln \frac{\Lambda^2}{m^2} - m^2 \text{li} \frac{\Lambda^2}{m^2} \right] + \frac{m^2}{4\pi} \left[\gamma_E - 1 - \ln \frac{\Lambda^2}{4m^2} \right] , \end{aligned}$$

with $\text{li}(x)$ denoting the logarithmic integral function.

However, at finite temperature numerical methods must be employed in order to calculate thermodynamical quantities. As was computed in [6, 7], the final result for the renormalised pressure to two-loop order at nonzero T is given by:

$$p_{\text{ren}}^{(2\text{-loop})} = \frac{N-2}{8\pi} (m_\phi^2 - M_\phi^2) + N \int_0^\infty \frac{dk k^2}{\pi} \frac{n[\omega_k(M_\phi)]}{\omega_k(M_\phi)} \quad (2.63)$$

$$+ \frac{NM_\phi^2}{2} \int_0^\infty \frac{dk}{\pi} \frac{n[\omega_k(M_\phi)]}{\omega_k(M_\phi)} + \frac{1}{2} \left[M_\phi^2 \frac{d(F_1 + F_2)}{dM_\phi^2} - F_1 - F_2 \right] .$$

Here F_1 is calculated using the Abel-Plana formula

$$F_1 = T \sum_{k_\tau=2\pi nT} \int_{-\infty}^{+\infty} \frac{dk}{2\pi} \ln G_\alpha^{-1}(K) - \int_{-\infty}^{+\infty} \frac{dk_\tau}{(2\pi)} \int_{-\infty}^{+\infty} \frac{dk}{(2\pi)} \ln G_\alpha^{-1}(K) , \quad (2.64)$$

and F_2 takes the form

$$F_2 = \mathcal{P} \int_K \ln \left[\frac{\tilde{G}_\alpha^{-1}(K)}{\ln(K^2/\tilde{M}^2)} \right] - \frac{M^2}{2\pi} \ln \ln \left(\frac{\Lambda^2}{\tilde{M}^2} \right) , \quad (2.65)$$

where \mathcal{P} indicates the principal value of the integral, and

$$G_\alpha^{-1}(K) \equiv \frac{1}{4\pi} \frac{\tilde{G}_\alpha^{-1}(K)}{\sqrt{K^2(K^2 + 4M^2)}} ; \quad (2.66)$$

$$\tilde{M}^2 = M^2 \exp \left[-4 \int_0^\infty \frac{dk}{\omega_k(M_\phi)} \frac{1}{\exp[\omega_k(M_\phi)/T] - 1} \right] . \quad (2.67)$$

Besides, M_ϕ is obtained by solving the equations

$$\frac{4\pi}{g_{\text{ren}}^2} = \left(1 - \frac{2}{N} \right) \ln \frac{\mu^2}{\overline{M}_\phi^2} + \frac{8}{N} \int_0^\infty \frac{dk}{\pi} \frac{1}{\omega_k(M_\phi)} \frac{1}{\exp[\omega_k(M_\phi)/T] - 1}$$

$$+ \frac{2}{N} \left[\ln 4 + 2\pi \frac{d(F_1 + F_2)}{dM_\phi^2} \right] ; \quad (2.68)$$

$$\overline{M}_\phi^2 = M_\phi^2 \exp \left[-4 \int_0^\infty \frac{dk}{\omega_k} \frac{1}{\exp[\omega_k/T] - 1} \right] . \quad (2.69)$$

These expressions will be used in Sec. 4 when comparing to the lattice results. Note that our results for the pressure to one- and two-loop order turn out to be *identical* to the ones of Ref. [6] in the $1/N$ expansion. This is a quite surprising result, which we discuss in more detail. Namely, in general the CJT formalism and the $1/N$ expansion are two different resummation prescriptions. The $1/N$ expansion corresponds to the large- N limit, whereas the CJT formalism is a loop expansion (moreover, the CJT formalism is applicable to systems out of equilibrium, which is not the case for the $1/N$ expansion).

Considering the case of 1+3 dimensions, one can show that in general these two resummation prescriptions give different results: to LO in the $1/N$ expansion there are N

degenerate (and, in the chiral limit, massless) pions and no massive sigma field is present, since this excitation only starts to propagate at NLO, see Ref. [27]. Conversely, in the CJT formalism in the one-loop approximation there are $N - 1$ massive pions and one massive sigma field, see Ref. [25]: this example demonstrates that the two methods are different (note that, if we perform the large N -limit *within* the one-loop order of the CJT method, there are N pions left. Thus, only if the large N limit is additionally applied does the one loop approximation of the CJT formalism give the same results as the LO in the $1/N$ expansion).

The fact that in two dimensions the results are equivalent, as shown in this work, is due to the absence of spontaneous symmetry breaking. Since the condensate is zero, the sigma and the pion become degenerate. This is equivalent to the large- N limit with N degenerate particles, which explains the agreement of our results with the LO approximation in $1/N$.

For the agreement at two loop order in 1+1 dimensions we were not able to get an analogous explanation: the two-loop result for the effective potential we obtain in Eq. (2.47) has a different expression from the one obtained in the $1/N$ expansion at NLO, which is equivalent to Eq. (2.61). Even after taking into account the absence of spontaneous symmetry breaking, one can not see directly the exact differences between the CJT formalism and the $1/N$ expansion. Only after taking the nonlinear limit, which is related to an infinitely large coupling constant, is it possible to perform some analytical simplifications, which allow us to rewrite the effective potential in such a way that it has the same form as the one in the $1/N$ expansion, Eq. (2.61). Moreover, what makes the comparison more difficult is the fact that we handle the bilinear propagator in a different way than the authors of Refs. [6, 7]. We eliminate the mixing term by a shift of the auxiliary field, while the authors of Refs. [6, 7] keep the mixing term and work with non-diagonal propagators.

Summarising, one can state that the exact determination of the differences between the CJT formalism and the $1/N$ expansion is a nontrivial task, which requires a detailed analytical study order by order. The two methods in general differ, since the leading orders in 1+3 dimensions are different; the fact that they coincide to leading order in 1+1 dimensions is also due to the peculiar dimensionality. The reason why they also coincide at two-loop order could not be clearly isolated, although we suspect that the lower dimensionality and the nonlinear limit play an important rôle. A further open question is whether this equivalence would persist at higher orders. While an explicit calculation is prohibitive, progress in this direction can be made if a formal way to connect the different methods is found.

3 Lattice simulation

In this Section we present the detailed evaluation of thermodynamical quantities of the $O(3)$ model by numerical lattice calculation. Some of the model's thermodynamic properties were studied in [35] in the context of the quest for a “perfect action”, free of discretisation systematics (see [36, 37]); a direct comparison to those findings seems however not to have an immediate significance, since there the fixed ratio $N_x/N_t = 3$ is maintained, while we choose to keep it well above 10 in all our simulations in order to suppress corrections to

the infinite-volume limit: this difference is important enough to alter the high-temperature asymptotic behaviour of p/T^2 , thereby invalidating any numerical comparison. Other than Ref. [35], to our knowledge no dedicated study of the thermodynamics has been performed on this model.

The Euclidean, discretised action under study takes the form of a Heisenberg model, i.e. an $O(3)$ spin model with nearest-neighbour interaction:

$$S = \beta \sum_{\langle i,j \rangle} (1 - \vec{s}_i \cdot \vec{s}_j) , \quad (3.1)$$

where the sum runs over all bonds of a 2-dimensional lattice and the \vec{s}_i are 3-dimensional unit vectors in internal space. The system at finite temperature T is realised by making the timelike extent of the lattice finite and consisting of N_t sites, with periodic boundary conditions in that direction: denoting with a the lattice spacing, we have $aN_t = 1/T$. The identification of the above action with the continuum one defining the partition function Eq. (2.1) is completed by setting $\beta = N/g^2$.

In a practical Monte Carlo simulation, moreover, the space extent of the lattice, N_x , is also necessarily finite; as long as $N_x \gg N_t$, however, this will hardly affect the temperature setting. In order to minimise the finite-size corrections, we will assume periodic boundary conditions in the spacelike direction throughout all of the following.

Our goal is to extract the thermodynamical behaviour of the action Eq. (3.1). In the next parts, the lattice methods will be illustrated along with the determination of the physical scale; subsequently, we present the numerical results that will later be compared to the predictions of the previous Section. A discussion of the algorithms implemented, their efficiency and autocorrelation is deferred to Appendix A.

3.1 Thermodynamical observables

For the evaluation of pressure p , trace anomaly θ and energy density ϵ , we adapt the “integral method” [38] to our (1+1)-dimensional model. We start from the continuum expression for the (nonphysical) pressure,

$$p_*(T) = T \frac{\partial \ln \mathcal{Z}}{\partial V} = \frac{T}{V} \ln \mathcal{Z} \quad (3.2)$$

(the second equality stems from the assumption of spatial isotropy, that always holds in the thermodynamic limit), where \mathcal{Z} is the partition function associated to S (it is understood that it refers to a system with timelike extent N_t):

$$\mathcal{Z} \propto \left(\prod_{\ell} \int_{S^2} d\vec{s}_{\ell} \right) \prod_{\langle i,j \rangle} e^{\beta \vec{s}_i \cdot \vec{s}_j} . \quad (3.3)$$

Since the one-dimensional spatial volume is given by $V = aN_x$, we have

$$a^2 p_*(T) = \frac{1}{N_x N_t} \ln \mathcal{Z} ; \quad (3.4)$$

we then write $\ln \mathcal{Z}$ as an integral in order to express it in terms of measurable quantities,

$$a^2 p_*(T) = \int_{\beta_0}^{\beta} d\beta' \frac{1}{N_x N_t} \frac{\partial \ln \mathcal{Z}}{\partial \beta} \Big|_{\beta'} ; \quad (3.5)$$

the integrand, exploiting translation invariance, has now become the expectation value of the energy per site,

$$\frac{1}{N_x N_t} \frac{\partial \ln \mathcal{Z}}{\partial \beta} = \langle \ell_x + \ell_t \rangle , \quad (3.6)$$

with the shorthand $\ell_e = \vec{s}_i \cdot \vec{s}_{i+\hat{e}}$. The last step is an additive renormalisation, needed to make the pressure finite: the standard choice is $p(T) = p_*(T) - p_*(0)$, which translates into the subtraction of the same integrand evaluated in a zero-temperature system (that is, $N_t = \infty$): making coupling and time extent explicit in the average values, we have then

$$\frac{p(T)}{T^2} = N_t^2 \int_0^{\beta} \left(\langle \ell_x + \ell_t \rangle_{\beta', N_t} - 2 \langle \ell \rangle_{\beta', \infty} \right) d\beta' . \quad (3.7)$$

In the above we fix the integration to start at $\beta_0 = 0$: on the practical side, this value can be directly simulated with no particular troubles.¹ Note also that $T = 0$ will be numerically approximated with a large enough square system, that is $N_x = N_t$.

Likewise, for the trace anomaly, starting from the continuum expression

$$\theta = T^3 \frac{\partial}{\partial T} \left(\frac{p}{T^2} \right) , \quad (3.8)$$

one derives

$$\frac{\theta(T)}{T^2} = N_t^2 \left(\frac{\partial \beta}{\partial \ln T} \right) \left(\langle \ell_x + \ell_t \rangle_{\beta, N_t} - 2 \langle \ell \rangle_{\beta, \infty} \right) . \quad (3.9)$$

This does not require integration over the coupling, but the knowledge of the beta-function is needed for the prefactor

$$\frac{\partial \beta}{\partial \ln T} = -a \frac{\partial \beta}{\partial a} . \quad (3.10)$$

The above will be extracted nonperturbatively, measuring the running of the coupling with the scale and using a suitable parametrisation of the resulting data.

Finally, we also consider the energy density

$$\epsilon = \frac{T^2}{V} \frac{\partial \ln \mathcal{Z}}{\partial T} = \theta + p . \quad (3.11)$$

3.2 Scale setting

The running of the scale $a(\beta)$ is needed to convert the temperature in physical units, as well as for the calculation of θ and ϵ . We evaluate it by computing, in a zero-temperature system and over a wide range of couplings, the spin-spin correlation function

$$C(an) = \langle \vec{s}_i \cdot \vec{s}_{i+n\hat{e}} \rangle , \quad (3.12)$$

¹It is in fact trivial and corresponds to generating all \vec{s}_i uniformly on the unit 2-sphere.

which then, to obtain the zero-temperature mass m , is fitted to the expected functional form for a two-dimensional scalar field, valid for large R :

$$C(R) \simeq c_0 \left(\frac{e^{-mR}}{\sqrt{mR}} + \frac{e^{-m(aN_x - R)}}{\sqrt{m(aN_x - R)}} \right) + c_1, \quad (3.13)$$

where we consider also the “mirror term” to account for the periodic boundaries. Distances on the lattice are in units of a , therefore the masses we measure are the adimensional quantities am ; once we fix the corresponding physical value we have the function $a(\beta)$ in units of $1/m$. The functional form Eq. (3.13), furthermore, is valid for large enough distances: in practice, we will fit the measurements to the function in a variable range $R_{\min} \leq R \leq R_{\max}$, looking for a plateau of the resulting am in R_{\min} . Furthermore, as the system never undergoes symmetry breaking, we expect the constant c_1 to vanish at all couplings in the infinite-volume limit.

3.3 Numerical results

3.3.1 Beta-function

The first task is the determination of the running of the scale. We measure the correlator Eq. (3.12) on lattices of size 156^2 and 256^2 for $\beta = 0.1, 0.2, \dots, 3.0$, generating 10^5 configurations for each setting, and use Eq. (3.13) to extract $am(\beta)$.

With the system volumes at our disposal, we can fit the data to Eq. (3.13) and find a satisfactory plateau for the mass in the region $\beta \lesssim 1.8$: beyond that value, the correlation length $\xi = 1/(am)$ grows too much, making our system size insufficient (Fig. 1, left); correspondingly, beyond that value the constant c_1 in Eq. (3.13) ceases to be compatible with zero. On the other hand, for couplings below $\beta \simeq 1.0$, the correlator signal drops too fast, i.e. the lattice becomes too coarse to measure the lightest mass of the theory.

The evaluation of the coefficient Eq. (3.10) is performed by locally interpolating the measured data as

$$\beta(a) = g_0 - g_1 a^\nu \quad (3.14)$$

and then differentiating the resulting curve; the interpolation is done on the 256^2 measurements, since a comparison with the 156^2 data shows that finite-size corrections are negligible. In this way we obtain the beta-function shown in Fig. 1 (right). The increasing difficulty in fixing the scale as β grows will be the main source of systematic error in the following results.

3.3.2 Thermodynamics

The integrand in Eq. (3.7) is evaluated on lattices with spatial sizes $N_x = 156$ and 256 , and all time extents $N_t = 6, \dots, 18$ for the finite-temperature part, plus the $N_t = N_x$ zero-temperature systems. We measure the average energy per site at all couplings $\beta' \leq \beta$ in steps of 0.1 and perform the integration evaluating the area under the curve², obtaining the pressure for $\beta = 1.0, 1.1, \dots, 1.7$, corresponding to lattice spacings in the range $0.02 \lesssim am \lesssim 0.55$.

²The integral was done using a simple trapezoid method. This gives satisfactory results since for the β stepsize which was used the curvature of $\ell(\beta)$ is very small.

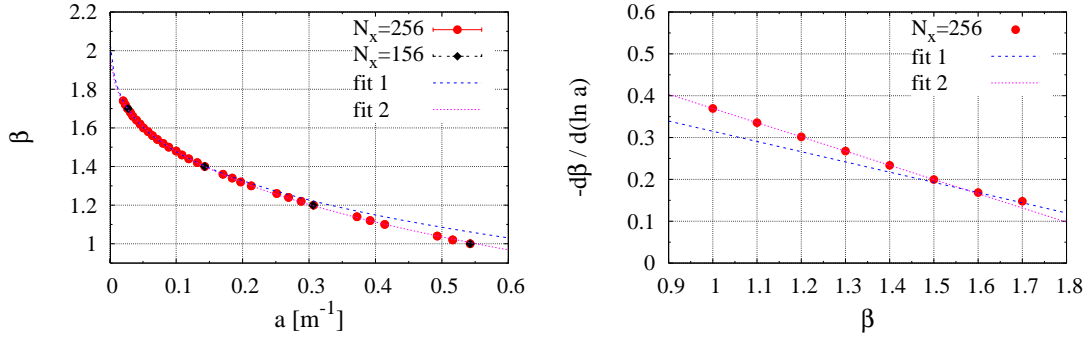


Figure 1. *Left:* the running coupling, computed on 156^2 and 256^2 lattices, with two parametrisations to the latter data, Eq. (3.14): fit 1 refers to $0.001 \leq am \leq 0.08$, while fit 2 is done in $0.01 \leq am \leq 0.6$. Error bars are much smaller than the symbol size; only some sample points are shown for the 156^2 lattice. *Right:* numerical results for the beta-function. Full circles indicate the final values used to set the physical scale.

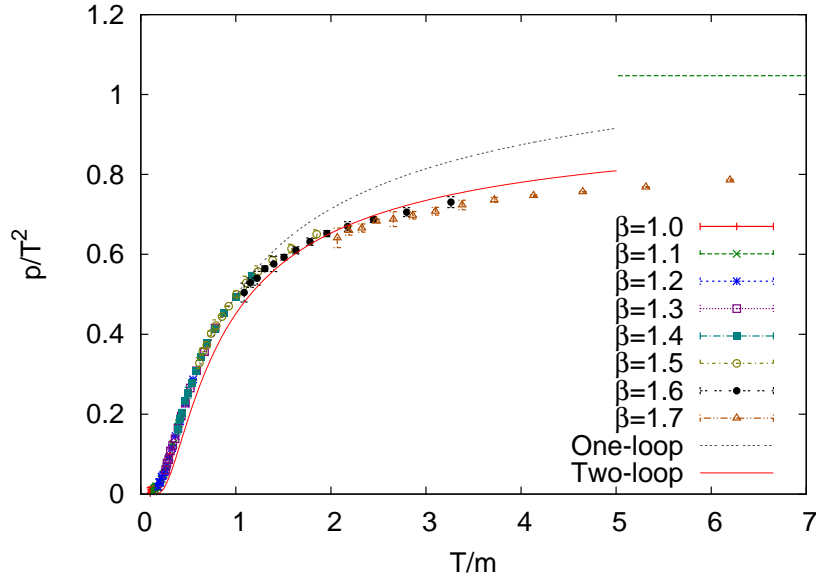


Figure 2. The physical pressure $p(T/m)/T^2$ from $N_x = 256$ systems at various lattice spacings. Each symbol represents a different (β, N_x) . Error bars show the systematic error from both discretisation and finite-size effects. The lines represent analytical calculations at LO and NLO (Eqs. (2.42) and (2.64), respectively); the horizontal line marks the asymptotic value $\frac{\pi}{3}$.

For each combination of N_t, N_x and β , 10^5 measurements were taken. The statistical error is estimated by binning the data in chunks of 1000, using Eq. (3.7) and averaging the resulting points for the physical pressure: it turns out that the uncertainties are very small and completely overcome by systematics.

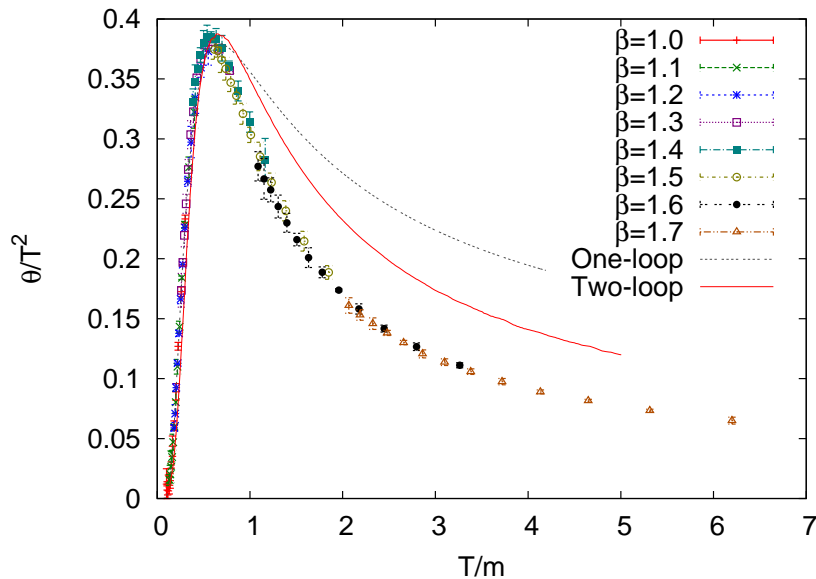


Figure 3. Trace anomaly $\theta(T/m)/T^2$; symbols are as in Fig. 2.

The results for p are plotted in Fig. 2, along with the analytical expectations. The slight differences between discretisations and system volumes are used to assess the systematic errors; however, the neat agreement between the various data sets is such that we consider both the thermodynamic and continuum limits to be effectively reached.

Similar considerations hold for the trace anomaly, calculated using the same input data through Eq. (3.9), and the energy density, obtained with Eq. (3.11). These are plotted in Figs. 3 and 4 respectively, along with the analytical predictions.

4 Comparison of analytical and lattice results

In this Section we compare the analytical results obtained in Sec. 2 with the lattice ones computed in Sec. 3 for the case $N = 3$. We organise this Section by first discussing pressure, trace anomaly, and energy density; then, we turn to two consequences of our study: the behaviour of the quasi-particle mass at nonzero temperature and the role of instantons/calorons in the thermodynamics.

Pressure. In Fig. 2 the pressure is plotted as function of T : we present the analytic curves at one- and two-loop order and the lattice points for different values of β . As one can deduce from the plot, the one-loop approximation describes well the lattice data for small temperatures. However, it overshoots them for large T . The pressure at two-loop level considerably improves the agreement of theory and lattice simulations for high T . Although a departure is still visible for increasing temperature, we can conclude that there is a good and parameter-free agreement between these two very different methods (the CJT formalism and lattice) of evaluating the pressure of the system.

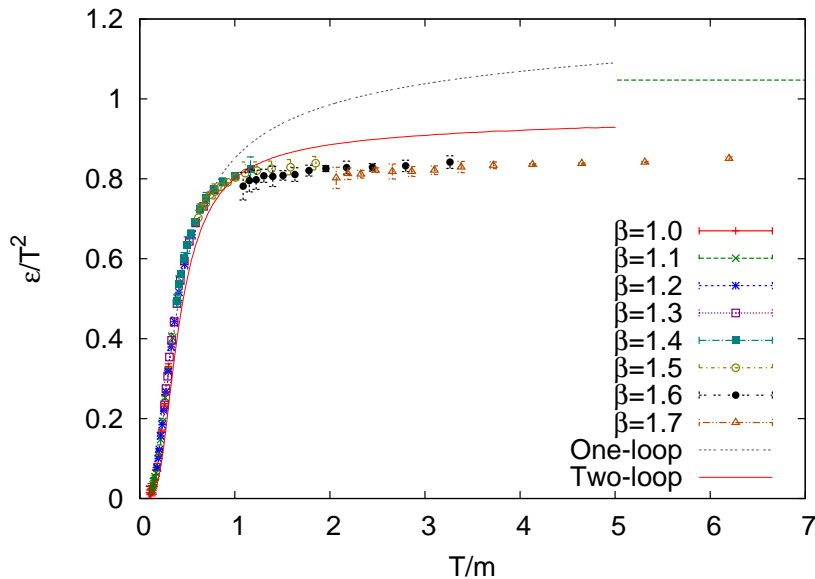


Figure 4. Energy density $\epsilon(T/m)/T^2$; symbols are as in Fig. 2.

Notice that this finding could be expected by a closer inspection of the properties of our analytic expressions: in fact, at one-loop level a good agreement with lattice data is not achievable because of a wrong asymptotic limit. Namely, in both cases the pressure approaches for high T the limit of a non-interacting gas of bosons, where each degree of freedom contributes as $\pi T^2/6$. However, at one-loop level there are, at high T , N active degrees of freedom, thus $p^{(1\text{-loop})}(T \gg m) = N\pi T^2/6$ for $T \rightarrow \infty$. This cannot be correct because the nonlinear constraint in Eq. (2.4) eliminates one degree of freedom. On the contrary, at the two-loop level one obtains the correct result $p^{(2\text{-loop})}(T \gg m) = (N-1)\pi T^2/6$ for $T \rightarrow \infty$, which shows that only $N-1$ non-interacting bosons are present, as it should be. This fact explains the much better agreement of the two-loop approximation at high temperature.

Trace anomaly. In Fig. 3 we present a similar plot of the function θ/T^2 . The apparent larger mismatch at high T relies on the fact that $\theta = \epsilon - p = T^3 \partial_T(p/T^2)$: the presence of a derivative enhances the disagreement for large T . However, it is very interesting to stress that both approaches show a form of the function θ/T^2 which looks very much like the one obtained in the deconfined phase of Yang-Mills theory, e.g. [38–40]. In fact, the present two-dimensional model, which does not have any phase transition, represents a simplified description of a gluonic gas above the critical temperature. Note that also in lattice simulations of Yang-Mills theories the maximum of the trace anomaly is reached above T_c just as our low-dimensional model does.

It is interesting to observe that θ grows linearly with T for large enough T . The lattice simulation shows that, for $T \gtrsim m$, the behavior $\theta \sim mT$ is realised: this simple power law may point to interesting features of the present theory. Also in four-dimensional

Yang-Mills theory the behaviour of the trace anomaly was studied: in Ref. [41] a quadratic behavior has been found. A similar finding has also been obtained in the analytical study of Ref. [42], whereas in Refs. [43, 44] a linear rise of the trace anomaly was determined. A deeper theoretical understanding of the behaviour of the trace anomaly would be surely important: the linear growth seen here for the simple $O(3)$ model may represent a suitable toy model for this purpose.

Energy density. In Fig. 4 we present the plot for the energy density. Analogous comments regarding the comparison of lattice and analytic results hold. Moreover, here it is clearly visible that the one-loop result overshoots the corresponding correct Boltzmann limit of $(N - 1)$ active DOFs in the high- T regime.

Quasi-particle mass. In the framework of our analytic approach we have calculated the mass of the particles as function of T . In Fig. 5 we plot the mass of the scalar particle $M(T)$ normalised to its vacuum value $M(0) = m$ as function of the temperature (notice that the mass $M(T)$ is the same for both the one-loop and the two-loop calculations). The function $M(T)$ starts from a nonzero value at $T = 0$ and then bends and reaches, as expected by basic dimensional consideration, a straight line for large T . This behaviour is reminiscent of that of the gluon mass in the deconfined phase of Yang-Mills theories [45–47]. The model exhibits dimensional transmutation just as QCD, meaning that at zero temperature there is a nonvanishing mass gap, which is generated due to renormalisation of quantum corrections. Note that the temperature at which the function $M(T)$ bends corresponds roughly to the maximum of the trace anomaly. Conversely, at high T the temperature-dependence of the mass can be approximately parametrised by $T/\log T$ in accordance with the aforementioned results concerning Yang-Mills theories.

Role of instantons. The $O(3)$ model in $1 + 1$ dimensions exhibits instantons in the vacuum and calorons at nonzero temperature. It is natural to ask if and how these topological objects affect thermodynamics. To this end, it should be stressed that the analytical method presented in Sec. 2 does not distinguish between trivial and nontrivial field configurations, neither in the vacuum nor at nonzero temperature. At a first sight, one may then argue that no instanton effects are present in our model: in fact, the method employed is valid for each N , while instantons are a peculiarity of the $N = 3$ case only. However, a closer inspection of our results is needed: namely, the system — as illustrated in Sec. 2 — shows nonperturbative properties: the vacuum is not realised by a constant value of the fields, such as $\sigma = \phi \neq 0$, rather by $\phi = 0$. Considering that the simple field configurations $\sigma = 0, \pi_i = 0$ is obviously not allowed (it violates the constraint), this means that rather complicated functions for $\sigma(x, \tau)$ and $\pi_i(x, \tau)$ with zero average are realised. For instance, an ensemble of calorons and anticalorons fulfills the required properties: all fields have zero average but nonzero contributions. We thus argue that the role of topological objects is prominent, because it naturally explains the nontrivial emergence of the vacuum $\langle \sigma \rangle = \langle \pi_i \rangle = 0$.

Indeed, in Ref. [23] the $O(3)$ model has been compared to the equivalent CP^1 model. In the case of CP^{n-1} models a calculation for the pressure was done only in the topologically

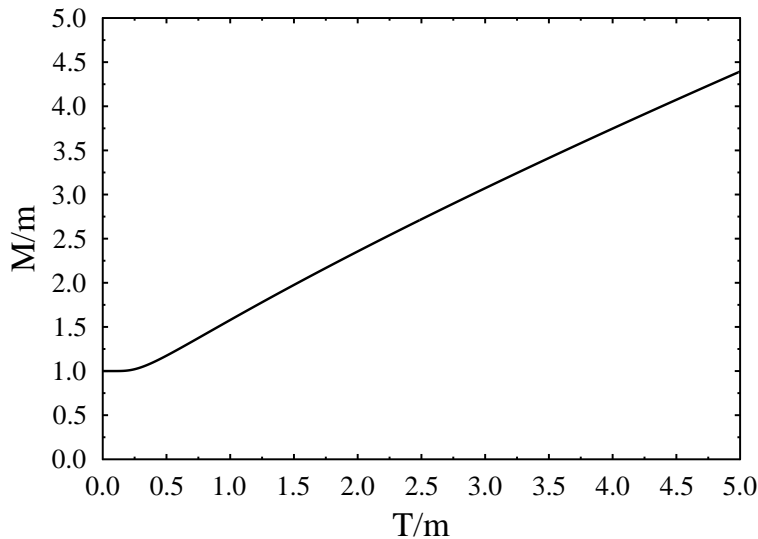


Figure 5. The quasi-particle mass $M(T)$ as function of T . For $T \rightarrow 0$ the constant value $M(0) = m$ is reached (dimensional transmutation). For high T the perturbative behaviour $M(T) \sim T/\ln(T)$ is realised.

trivial sector: in fact, in that case it was possible to distinguish between the different topological sectors of the theory. A comparison of the pressure of the CP^1 model with that of the $O(3)$ model shows a large discrepancy, which was ascribed to instanton/caloron effects by the authors of Ref. [23]. Obviously, this conclusion holds only under the assumption that the instanton contributions are indeed included in the thermodynamical treatment of the $O(3)$ model. As we argue above, this seems to be the case.

In this context, it is interesting to observe that the lattice data show a linear growth of the trace anomaly with the temperature. This feature implies a nonperturbative bag pressure which also grows linearly with T : in Ref. [44] this linear behaviour of the trace anomaly has been linked to a ground state dominated by caloron/anticaloron fluctuations. Thus, a direct calculation of the instanton/caloron role in the $O(3)$ model would be very desirable from both the analytic and the lattice sides. Moreover, the $O(3)$ calorons contain also monopole constituents, just as Yang-Mills theories [16]. An estimate of the contributions of these constituents to thermodynamics would also be very interesting.

5 Summary

In this work we have studied the thermodynamics of the $O(N = 3)$ model in 1+1 dimensions using the CJT formalism and the auxiliary field method to one- and two-loop orders. At the same time, we have performed a precise lattice simulation for this system at nonzero temperature applying the integral method.

Our main results are displayed in Figs. 2, 3 and 4 where the theoretical curves have been compared to the lattice calculation. It should be stressed that, once the mass of

the field in the vacuum is used as an energy unit, no free parameters in the analytical calculation are present: the agreement shown in the aforementioned figures confirms the power of the employed analytic formalism. In particular, at one-loop level the results are very good for small temperature, but not so at large T because of an expected failure in this energy domain. Namely, in this approximation a gas of free N bosons is realised in this limit, while only $N - 1$ degrees of freedom exist due to the nonlinear constraint entering the definition of the model. At two-loop order this problem is solved and the correct asymptotic limit is reached. The agreement of theory and lattice is therefore much better in the high- T domain. Surely, theoretical improvement can still be done in order to achieve an even better matching.

The $O(N)$ model is very interesting because it shares some properties with Yang-Mills theory, such as trace anomaly and asymptotic freedom. In fact, the form of the trace anomaly (see Fig. 3) shows a striking analogy to the more difficult four-dimensional Yang-Mills case. For these reasons the lattice results presented here can be of interest for testing other theoretical methods dealing with nonperturbative features of quantum field theory. Namely, while going beyond the two-loop CJT results presented in this work would be a very hard technical task, one could develop new theoretical methods which involve new resummation schemes. Surely, a better understanding of such methods in a model which shares many similarities with Yang-Mills gauge systems can be of great use to improve our knowledge on the latter.

A further interesting achievement has been the determination of the temperature-dependent mass $M(T)$, see Fig. 5. Also in this case a form which is reminiscent of that of the gluon mass in the deconfined phase of Yang-Mills systems is obtained: for small T one has $M(T) \simeq m \neq 0$ (dimensional transmutation), while for large T one has the expected perturbative growth $M(T) \sim T/\ln T$.

For the particular choice $N = 3$ used in this work the $O(3)$ model contains also instantons. We have argued that these topological configurations, although not explicitly included in our evaluation, are anyhow present because they naturally generate the nontrivial vacuum of the system. Indeed, a further study in this direction represents an interesting outlook both as an analytic and as a lattice study of the $O(3)$ system.

One can also include in the present model a so-called θ -term which mimics the axial anomaly of QCD (see for instance [48]): a thermodynamical investigation of this system is feasible both analytically and numerically.

We also mention the possibility of a comparison between the results presented here and an analysis based on a thermodynamic Bethe Ansatz adjusted to the model under study.

Acknowledgements

The authors would like to thank Harmen Warringa for his precious help, suggestions and discussions in the analytical part of this work. The authors thank also Dirk H. Rischke, Owe Philipsen, Stefan Schramm, Rob Pisarski, Hendrik van Hees, Tomas Brauner and Ralf Hofmann for valuable discussions and a critical reading of the manuscript. The nu-

merical simulations presented here were performed at the Center for Scientific Computing (CSC) at Frankfurt University. This work has been partly supported through the Helmholtz International Center for FAIR which is part of the Landes-Offensive zur Entwicklung wissenschaftlich-ökonomischer Exzellenz (LOEWE) of the state of Hesse. F.G. acknowledges financial support from the Politechnical Society of Frankfurt/M. through an Educator fellowship.

A Algorithms and autocorrelations

We now come to a study and comparison of the various algorithms that can be implemented to investigate numerically the model, Eq. (3.1). Aside from the ordinary, quite inefficient Metropolis algorithm, which we use only for cross-checking purposes, we tested the heatbath update method, the cluster method and the microcanonical overrelaxation.

In the following we measure and compare the most important indicator of an algorithm’s efficiency, namely the (integrated) autocorrelation time τ_{int} , which measures how many elementary update steps are needed to generate a new, statistically uncorrelated configuration while exploring the phase space of the theory through the Markov chain driven by the update method. Furthermore, the final measure of the efficiency of an algorithm is not τ_{int} itself (measured in numbers of updates), but rather τ_{int}^{real} (measured in seconds), the product of τ_{int} and the average wallclock time it takes, on a given machine, to perform a single update (which, in particular for cluster-based methods, may largely depend on the coupling). All simulations presented in this work have been done on individual cores of AMD Opteron 2427 (Istanbul) CPUs with a clock rate of 2211 MHz. No parallelisation has been employed.

In general, different autocorrelations are associated to different observables. We focus on three quantities: two are of obvious physical interest, corresponding to the energy- and ordering-like relevant scaling operators, which are general for $O(N)$ models,

$$e = \frac{\left\langle \sum_{\langle i,j \rangle} (1 - \vec{s}_i \cdot \vec{s}_j) \right\rangle}{2N_x N_t}, \quad m = \frac{\left\langle \left| \sum_{\ell} \vec{s}_{\ell} \right| \right\rangle}{N_x N_t}. \quad (\text{A.1})$$

The third one is the volume-average of a single component of the \vec{s}_i and gives a measure for “isotropy-like” correlations, i.e. a memory of prior global direction in internal space,

$$i = \frac{\left\langle \sum_k \vec{s}_k \cdot \hat{e}_1 \right\rangle}{N_x N_t}. \quad (\text{A.2})$$

Its autocorrelation, which is technically interesting and can in fact become quite large (where the system has large spatial correlations), is however for the most part irrelevant from the quantum field theory perspective, which is concerned primarily with $O(3)$ -symmetric physics.

To estimate the autocorrelation, one can employ a binning analysis with bins of variable size [49], or use the jackknife method; here, we apply the more refined technique proposed in [50]. All autocorrelation measurements have to be made after thermalisation is reached,

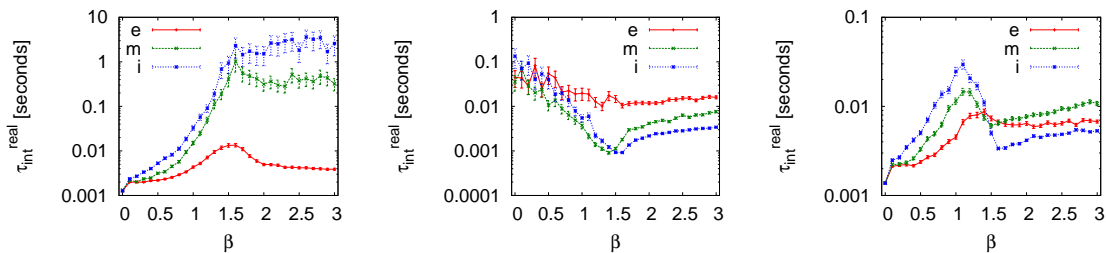


Figure 6. Real-time $\tau_{\text{int}}^{\text{real}}$ from simulations on a 64^2 lattice, for heatbath (left), Wolff (middle) and mixed (right) update methods. Note the semi-logarithmic scale.

which in the present case is determined by inspection of the Monte Carlo time histories for the observables defined above.

In the following we discuss the algorithms we implemented in terms of their τ_{int} and $\tau_{\text{int}}^{\text{real}}$, and present the mixed strategy we adopted for all simulations reported in Subsection 3.3, which ensures efficiency over the whole β -range of interest.

Heatbath

The model, Eq. (3.1), is suited for the heatbath update. The new vector on site i is extracted randomly according to the equilibrium probability distribution induced by the associated contribution to the action, involving its four neighbours:

$$P(\vec{s}_i) \sim \exp \left[\beta \vec{s}_i \cdot \left(\sum_{\hat{\nu}=\pm\hat{e}_j} \vec{s}_{i+\hat{\nu}} \right) \right] \quad (\text{A.3})$$

In practice, it amounts to generating the angle between the sum vector and the new \vec{s}_i according to the above formula, and then uniformly choosing a random azimuthal angle [49].

All sites of the lattice are updated in a checkerboard fashion: this constitutes an update step (“sweep”). In Fig. 6 (left) the behaviour of $\tau_{\text{int}}^{\text{real}}$ for the three observables on a 64^2 lattice is shown (we focus on this quantity instead of τ_{int} to make a meaningful comparison between different update methods, however for the heatbath update the two are proportional in a β -independent way). It is apparent that the method, while performing well for small couplings, suffers from the long-range correlations that develop as $\beta \gtrsim 1$, especially for the ordering-like operators: there, alternative methods should be considered.

Cluster algorithm

We then test the cluster update method, developed by Wolff [51] generalising the work of Swendsen and Wang [52] for the Ising model. The idea is to build clusters of spins, reflecting to some extent the structures, in the system, which carry the long-range correlations, and update these clusters all at once. For our model, an update step consists of the following operations:

- a) Choose a random site x_i and a random reflection plane π with surface normal \hat{n} (“seeding”). Reflect \vec{s}_i across π and mark x_i .
- b) Examine all nearest neighbours $\{x_j\}$ of x_i and with probability
$$p = 1 - \exp\{\min[0, 2\beta(\hat{n} \cdot \vec{s}_i)(\hat{n} \cdot \vec{s}_j)]\}$$
reflect \vec{s}_j across π and mark x_j as well.
- c) Repeat step b) for all links connecting newly marked sites to unmarked neighbours until the process stops.

Clustering methods are generally understood to be free of critical slowing down: thus, they are suitable for simulations in the vicinity of a critical point. Our model does not exhibit a true transition in two dimensions, nevertheless we implement the Wolff algorithm and investigate its efficiency, since on any finite volume we see a strong ordering tendency at large enough couplings.

The average size of a cluster (therefore, the time needed perform a single update) grows with β : indeed, we observe it increases by more than an order of magnitude between $\beta = 0.1$ and $\beta = 3.0$. This is, however, completely countered by a shortening of the autocorrelation as the clusters span a larger portion of the system, so that, in terms of $\tau_{\text{int}}^{\text{real}}$, the efficiency of this algorithm in disordering the configuration is generally better at larger couplings (Fig. 6, middle). In the region of small β , the heatbath is still superior than this method, so in the following we devise a mixed update that ensures small autocorrelation over the whole range of couplings under study.

The mixed strategy

Based on the findings presented so far, we expect that a judicious combination of the two algorithms would perform well at all couplings. We then define from now on an “update sweep” as the combination of a single heatbath sweep throughout the lattice combined with ten cluster seedings.

Fig. 6 (right) shows the resulting $\tau_{\text{int}}^{\text{real}}$ on a 64^2 system: this update is indeed more efficient than either heatbath or cluster alone over the whole β range. Hence, we use the mixed strategy for the thermodynamical investigation presented in Subsection 3.3.

We now turn to the question of the scaling of τ_{int} with the system volume for the mixed update: this is useful for a proper tuning of the Monte Carlo data taking based on the size of the lattice under study. We measure τ_{int} in units of sweeps, as defined above, on various square systems with size up to $N_x = 64$ for energy- and ordering-like observables; these are plotted in Fig. 7. The latter seems always to be a bit slower to decorrelate, so we base our tuning on its behaviour. It turns out that the height peak of $\tau_{\text{int}}(\beta)$, located roughly at $\beta \sim 1.2$, can be described as a function of the system size with a power law:

$$\tau_{\text{int}}^*(N_x) \simeq aN_x^{2b} \quad , \quad a = 0.13(5) \quad , \quad b = 0.38(6) \quad , \quad (\text{A.4})$$

this implies the upper bounds $\tau_{\text{int}}^*(156) \sim 6$ and $\tau_{\text{int}}^*(256) \sim 9$; to be on the safe side, in collecting the data of Subsection 3.3, we perform respectively 14 and 21 sweeps between measurements.

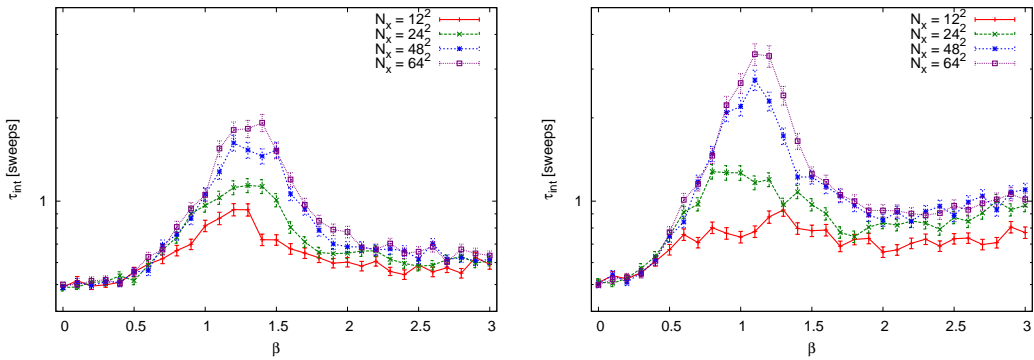


Figure 7. τ_{int} as a function of the coupling for the mixed update on square systems of various sizes, for the e (left) and the m (right) observables. Note the semi-logarithmic scale.

Metropolis and overrelaxation

For the purpose of cross-checking, we also implemented a standard Metropolis update, where a proposed new value of \vec{s}_i is accepted with probability $p = \min[1, \exp(-\Delta S)]$, with ΔS the corresponding change in the action. The associated autocorrelation is qualitatively similar to the heatbath procedure, but it is about an order of magnitude larger than the latter.

We also investigated whether the algorithm's efficiency can be improved with micro-canonical overrelaxation, i.e. a random rotation of \vec{s}_i about the sum of the neighbours' spins so to achieve maximum disordering of the configuration while exactly preserving the energy and the Metropolis acceptance. While this brings indeed the Metropolis update to an efficiency comparable to the heatbath in the region $\beta \gtrsim 1$, we do not see any gain at lower couplings: therefore, we refrain from exploring this avenue any further.

References

- [1] A. M. Polyakov, *Interaction of Goldstone Particles in Two-Dimensions. Applications to Ferromagnets and Massive Yang-Mills Fields*, Phys. Lett. B **59** (1975) 79.
- [2] V. A. Novikov, M. A. Shifman, A. I. Vainshtein and V. I. Zakharov, *Two-Dimensional Sigma Models: Modeling Nonperturbative Effects of Quantum Chromodynamics*, Phys. Rept. **116**, 103 (1984) [Sov. J. Part. Nucl. **17**, 204 (1986)] [Fiz. Elem. Chast. Atom. Yadra **17**, 472 (1986)].
- [3] C. Rim and W. I. Weisberger, *Ultraviolet Divergences In The $1/n$ Expansion Of The Scalar $O(n)$ Model*, ITP-SB-84-16.
- [4] H. Flyvbjerg, *Scaling Versus Asymptotic Scaling In The Nonlinear Sigma Model In 2-d: Continuum Version*, Phys. Lett. B **245**, 533 (1990).
- [5] D. J. Gross, R. D. Pisarski and L. G. Yaffe, *QCD and Instantons at Finite Temperature*, Rev. Mod. Phys. **53**, 43 (1981).
- [6] J. O. Andersen, D. Boer and H. J. Warringa, *Thermodynamics of the $O(N)$ nonlinear sigma model in $(1+1)$ -dimensions*, Phys. Rev. D **69**, 076006 (2004) [hep-ph/0309091].

- [7] H. J. Warringa, *Thermodynamics of the 1+1-dimensional nonlinear sigma model through next-to-leading order in 1/N*, hep-ph/0408257.
- [8] M. Shifman and A. Yung, *Non-Abelian Confinement in $N=2$ Supersymmetric QCD: Duality and Kinks on Confining Strings*, Phys. Rev. D **81** (2010) 085009 [arXiv:1002.0322 [hep-th]].
- [9] N. D. Mermin and H. Wagner, *Absence of ferromagnetism or antiferromagnetism in one-dimensional or two-dimensional isotropic Heisenberg models*, Phys. Rev. Lett. **17**, 1133 (1966).
- [10] S. R. Coleman, *There are no Goldstone bosons in two-dimensions*, Commun. Math. Phys. **31**, 259 (1973).
- [11] R. G. Root, *Effective Potential for the $O(N)$ Model to Order $1/N$* , Phys. Rev. D **10**, 3322 (1974).
- [12] P. Biscari, M. Camprostrini and P. Rossi, *Quantitative Picture Of The Scaling Behavior Of Lattice Nonlinear Sigma Models From The $1/n$ Expansion*, Phys. Lett. B **242**, 225 (1990).
- [13] M. Dine and W. Fischler, *The Thermodynamics Of The Nonlinear Sigma Model: A Toy For High Temperature Qcd*, Phys. Lett. B **105**, 207 (1981).
- [14] J. M. Cornwall, R. Jackiw and E. Tomboulis, *Effective Action for Composite Operators*, Phys. Rev. D **10**, 2428 (1974).
- [15] F. Bruckmann, *Topological objects in QCD*, Eur. Phys. J. ST **152**, 61 (2007) [arXiv:0706.2269 [hep-th]].
- [16] F. Bruckmann, *Instanton constituents in the $O(3)$ model at finite temperature*, Phys. Rev. Lett. **100**, 051602 (2008) [arXiv:0707.0775 [hep-th]].
- [17] H. Eichenherr, *$SU(N)$ Invariant Nonlinear Sigma Models*, Nucl. Phys. B **146**, 215 (1978) [Erratum-ibid. B **155**, 544 (1979)].
- [18] R. Banerjee, *Quantum equivalence of $O(3)$ nonlinear sigma model and the CP^{*1} model: A Gauge independent Hamiltonian approach*, Phys. Rev. D **49**, 2133 (1994).
- [19] Schafer and E. V. Shuryak, *Instantons in QCD*, Rev. Mod. Phys. **70** (1998) 323 [hep-ph/9610451].
- [20] R. Hofmann, *Nonperturbative approach to Yang-Mills thermodynamics*, Int. J. Mod. Phys. A **20** (2005) 4123 [hep-th/0504064];
- [21] U. Herbst and R. Hofmann, *Asymptotic freedom and compositeness*, ISRN High Energy Phys. **2012** (2012) 373121 [hep-th/0411214];
- [22] F. Giacosa and R. Hofmann, *Thermal ground state in deconfining Yang-Mills thermodynamics*, Prog. Theor. Phys. **118** (2007) 759 [hep-th/0609172].
- [23] J. O. Andersen, D. Boer and H. J. Warringa, *The Effects of quantum instantons on the thermodynamics of the $CP^{*(N-1)}$ model*, Phys. Rev. D **74** (2006) 045028 [hep-th/0602082].
- [24] G. Fejos, A. Patkos and Z. Szep, *Renormalized Phi-functionals for the $O(N)$ model at next-to-leading order of the $1/N$ expansion*, Phys. Rev. D **80**, 025015 (2009) [arXiv:0902.0473 [hep-ph]].
- [25] E. Seel, S. Struber, F. Giacosa and D. H. Rischke, *Study of Chiral Symmetry Restoration in Linear and Nonlinear $O(N)$ Models using the Auxiliary Field Method*, Phys. Rev. D **86**, 125010 (2012) [arXiv:1108.1918 [hep-ph]].

- [26] J. T. Lenaghan and D. H. Rischke, *The $O(N)$ model at finite temperature: Renormalization of the gap equations in Hartree and large N approximation*, J. Phys. G G **26** (2000) 431 [nucl-th/9901049].
- [27] S. Borsanyi and U. Reinosa, *The Pressure of QED from the two-loop 2PI effective action*, Phys. Lett. B **661**, 88 (2008) [arXiv:0709.2316 [hep-ph]].
- [28] J. Berges, S. Borsanyi, U. Reinosa and J. Serreau, *Renormalized thermodynamics from the 2PI effective action*, Phys. Rev. D **71**, 105004 (2005) [hep-ph/0409123].
- [29] N. Petropoulos, *Linear sigma model and chiral symmetry at finite temperature*, J. Phys. G **25**, 2225 (1999) [J. Phys. G G **25**, 2225 (1999)] [hep-ph/9807331].
- [30] M. Grahl, E. Seel, F. Giacosa and D. H. Rischke, *The $O(2)$ model in polar coordinates at nonzero temperature*, arXiv:1110.2698 [nucl-th].
- [31] H. van Hees and J. Knoll, *Renormalization in selfconsistent approximation schemes at finite temperature. 3. Global symmetries*, Phys. Rev. D **66** (2002) 025028 [hep-ph/0203008].
- [32] G. Amelino-Camelia, *Thermal effective potential of the $O(N)$ linear sigma model*, Phys. Lett. B **407** (1997) 268 [hep-ph/9702403].
- [33] F. Cooper, J. F. Dawson and B. Mihaila, *Renormalized broken-symmetry Schwinger-Dyson equations and the 2PI-1/N expansion for the $O(N)$ model*, Phys. Rev. D **71**, 096003 (2005) [hep-ph/0502040].
- [34] J. O. Andersen, D. Boer and H. J. Warringa, *Thermodynamics of $O(N)$ sigma models: 1/N corrections*, Phys. Rev. D **70**, 116007 (2004) [hep-ph/0408033].
- [35] S. Spiegel, *Thermodynamics of the two-dimensional $O(3)$ sigma model with fixed point lattice action*, Phys. Lett. B **400**, 352 (1997) [hep-lat/9611027].
- [36] P. Hasenfratz and F. Niedermayer, *Perfect lattice action for asymptotically free theories*, Nucl. Phys. B **414**, 785 (1994) [hep-lat/9308004];
- [37] P. Hasenfratz, *Prospects for perfect actions*, Nucl. Phys. Proc. Suppl. **63**, 53 (1998) [hep-lat/9709110].
- [38] G. Boyd, J. Engels, F. Karsch, E. Laermann, C. Legeland, M. Lutgemeier and B. Petersson, *Thermodynamics of $SU(3)$ Lattice Gauge Theory*, Nucl. Phys. B **469** (1996) 419 [arXiv:hep-lat/9602007].
- [39] M. Panero, *Thermodynamics of the QCD plasma and the large- N limit*, Phys. Rev. Lett. **103** (2009) 232001 [arXiv:0907.3719 [hep-lat]].
- [40] S. Borsanyi, G. Endrodi, Z. Fodor, S. D. Katz and K. K. Szabo, *Precision $SU(3)$ lattice thermodynamics for a large temperature range*, JHEP **1207**, 056 (2012) [arXiv:1204.6184 [hep-lat]].
- [41] R. D. Pisarski, *Fuzzy Bags and Wilson Lines*, Prog. Theor. Phys. Suppl. **168** (2007) 276 [hep-ph/0612191].
- [42] F. Giacosa, *Analytical study of a gas of gluonic quasiparticles at high temperature: Effective mass, pressure and trace anomaly*, Phys. Rev. D **83** (2011) 114002 [arXiv:1009.4588 [hep-ph]];
- [43] D. E. Miller, *Lattice QCD Calculation for the Physical Equation of State*, Phys. Rept. **443** (2007) 55 [hep-ph/0608234].
- [44] F. Giacosa and R. Hofmann, *Linear growth of the trace anomaly in Yang-Mills thermodynamics*, Phys. Rev. D **76** (2007) 085022 [hep-th/0703127].

- [45] F. Brau and F. Buisseret, *Glueballs and statistical mechanics of the gluon plasma*, Phys. Rev. D **79** (2009) 114007 [arXiv:0902.4836 [hep-ph]];
- [46] A. Peshier, B. Kampfer, O. P. Pavlenko and G. Soff, *A Massive quasiparticle model of the $SU(3)$ gluon plasma*, Phys. Rev. D **54** (1996) 2399;
- [47] P. Castorina and M. Mannarelli, *Effective degrees of freedom and gluon condensation in the high temperature deconfined phase*, Phys. Rev. C **75** (2007) 054901 [hep-ph/0701206 [hep-ph]].
- [48] D. Nogradi, *An ideal toy model for confining, walking and conformal gauge theories: the $O(3)$ sigma model with theta-term*, JHEP **1205**, 089 (2012) [arXiv:1202.4616 [hep-lat]].
- [49] B. A. Berg, *Markov chain Monte Carlo simulations and their statistical analysis*, World Scientific, 2004.
- [50] U. Wolff [ALPHA Collaboration], *Monte Carlo errors with less errors*, Comput. Phys. Commun. **156**, 143 (2004) [Erratum-ibid. **176**, 383 (2007)] [hep-lat/0306017].
- [51] U. Wolff, *Collective Monte Carlo Updating for Spin Systems*, Phys. Rev. Lett. **62**, 361364 (1989).
- [52] R. H. Swendsen and J. -S. Wang, *Nonuniversal critical dynamics in Monte Carlo simulations*, Phys. Rev. Lett. **58**, 86 (1987).